Transition matrix elements for μ-e conversion in ^{72}Ge using the deformed Hartree-Fock method

T. S. Kosmas
Theoretical Physics Division, University of Ioannina, GR-45110 Ioannina, Greece

Amand Faessler and R. Sahu*
Institut für Theoretische Physik der Universität Tübingen, D-72076 Tübingen, Germany
(Received 5 May 2003; published 24 November 2003)

The low-lying spectrum of $^{72}_{32}$Ge nucleus is constructed in the context of a deformed configuration mixing shell model approach based on Hartree-Fock states. We use as two-body interaction the modified Kuo effective-interaction for the $f_{5/2}pg_{9/2}$ valence space. Subsequently, the matrix elements for transitions to low-lying excitations induced by the exotic μ-e conversion operators on this isotope are calculated. This study is, among other reasons, motivated by the recent estimations on the $\mu^- \rightarrow e^-$ branching ratio, $R_{\mu e}(A,Z)$, which have shown that $R_{\mu e}$ becomes maximum for $Z \approx 30-60$, a region of the periodic table that includes the Ge isotopes.

DOI: 10.1103/PhysRevC.68.054315 PACS number(s): 23.40.Bw, 13.35.Bv, 21.60.Jz, 12.60.Cn

I. INTRODUCTION

The muon-electron conversion in nuclei, $(A,Z)+\mu_b^- \rightarrow e^- + (A,Z)^*$, is an important and challenging electroweak process [1–3] which violates the conservation of lepton-flavor quantum numbers L_μ and L_e by one unit. Recently, it has been the subject of considerable theoretical [2,4,5] and experimental [6–10] work. From the experimental attempts performed with the objective to "measure" the branching ratio $R_{\mu e}$ of this process, stringent limits on the lepton-flavor violation (LFV) parameters have been obtained while significant improvements over these limits are expected in the near future by the new μ-e conversion experiments, i.e., SINDRUM II at PSI [6,7], MECO at BNL [8,9], and PRIME at KEK [10]. On the other hand, the formulation of the $\mu^- \rightarrow e^-$ nucleon-level Lagrangian has been done [11] in terms of the nucleon effective fields in a Lorentz covariant form where all possible types of interactions—(pseudo)scalar, (axial)vector and tensor—are included. Furthermore, the one-body nuclear matrix elements of the basic nuclear-level operators resulting from this Lagrangian have been compactly formulated [12] and the many-body nuclear wave functions (with definite spin and parity) describing the low-lying nuclear excitations induced by the $\mu^- \rightarrow e^-$ operators have been deduced in the context of some nuclear methods [shell model, quasiparticle random phase approximation (QRPA), renormalized QRPA, etc.] for various nuclei [13–16].

Recently, it was argued that several from the aforementioned nuclear structure methods, mostly used to investigate nuclear matrix elements for many electroweak processes, rely upon symmetry violating model Hamiltonians [17–19], i.e., Hamiltonians for which symmetries such as the translational and rotational invariance, the particle number conservation, the Pauli exclusion principle, etc., are not satisfactorily fulfilled. As a result, spurious contaminations are inserted into the produced nuclear spectrum (e.g., the 0^+, 1^-, etc.). In some processes, such as the $\beta\beta$-decay, μ-e conversion, etc., a great part of the transition strength is predicted to proceed via such excitations, so that the restoration of the broken symmetries and the subsequent elimination of the spurious admixture inserted into the calculated spectrum is required [17–19]. In addition, the nuclear deformation (e.g., for axially symmetric nuclear systems) should necessarily be considered by applying appropriate treatments and using reliable methods.

The present paper, in addition to the above arguments, is also motivated by the conclusions of the recent calculations carried out for studying the nuclear structure dependence of the branching ratio $R_{\mu e}(A,Z)$ throughout the periodic table [20]. These results have shown that the coherent ratio $R_{\mu e}$ becomes maximum when $Z \approx 30-60$, a conclusion that may be helpful in choosing the appropriate target nuclei for future μ-e conversion experiments. In spite of the fact that the incoherent (μ^-, e^-) rate (not estimated in Ref. [20] and much harder to be calculated) is less significant portion of the total rate, however, it is important for estimating the experimentally interesting quantity of the ratio of the coherent to the total (μ^-, e^-) rate. This quantity needs reliable calculations for both coherent and incoherent nuclear strengths. As is well known, the incoherent branching ratio can be experimentally estimated by taking the difference between the measured and Monte Carlo muon decay-in-orbit $(\mu^- \rightarrow e^- \nu\bar{\nu})$ spectra [6]. Theoretically, this rate can be explicitly evaluated by constructing the excited nuclear states included in a chosen model space.

The region of the periodic table with $Z \approx 30-60$ includes the Ge ($Z=32$) isotopes (the most abundant are ^{70}Ge 21.2%, ^{72}Ge 27.7%, and ^{74}Ge 35.9%). In the present work, we take this advantage, first, to construct the low-lying spectrum of the rather deformed $^{72}_{30}$Ge nucleus (it presents moderate deformation having quadrupole deformation-parameter $\beta_2 = -0.214$) by using the deformed Hartree-Fock (DHF) method [21–23], and, second, to calculate its incoherent and coherent (μ^-, e^-) transition matrix elements. This method provides, in general, a good description of the low-lying

*Permanent address: Physics Department, Berhampur University, Berhampur 760007, India.

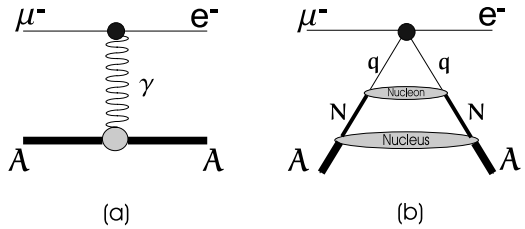

FIG. 1. Diagrams contributing to $\mu^- \to e^-$ conversion: (a) Photon exchange, and (b) four-fermion contact interaction (nonphotonic mechanisms) mediated by heavy particles (*W* bosons, Higgs particles, *s*-fermion, etc.).

spectroscopic properties of even-even, odd-even, and odd-odd nuclear systems and over the last two decades it has been applied to several nuclei in the $A \approx 60-100$ region [21–23]. The restoration of some symmetry violations, mentioned before, in the DHF method may automatically be incorporated. Moreover, the DHF method, by employing as two-body interaction a modified Kuo effective interaction in the $f_{5/2}pg_{9/2}$ active space, has good success in analyzing the band structures seen in many ($N \neq Z$) nuclei, such as even-even isotopes of Ge, Kr, Sr, etc. [21]. This means that, the nuclear wave functions of the DHF are well tested and the confidence level of the obtained results may be high in a region where the ratio $R_{\mu e}$ takes the largest value [20]. In view of these events, it would be interesting to examine the predictions of the DHF regarding the exotic μ-*e* conversion matrix elements (coherent and incoherent) in the ^{72}Ge isotope and compare them with the existing results obtained by single Slater determinant calculations (closure approximation) [24], and results obtained by using RPA methods [16]. We remark that, in the sets of nuclei of these studies [16,20,24] only ^{72}Ge from the Ge isotopes is included.

The paper, is organized as follows. In Sec. II, we present in brief the formalism, first, for the $\mu \to e$ conversion nuclear-level operators and then for their transition matrix elements within the deformed HF method. The calculated spectrum of ^{72}Ge and the μ-*e* conversion transition matrix elements are presented and compared with previous results in Sec. III, and finally (Sec. IV) the extracted conclusions are summarized.

II. FORMALISM OF $\mu^- \to e^-$ TRANSITION MATRIX ELEMENTS IN THE DHF

A. The basic nuclear-level operators

In order to write down at nuclear level the relevant operators describing the assumed $\mu^- \to e^-$ mechanism, one starts from a nucleon-level Lagrangian. Here we use the general effective Lagrangian written in a Lorentz covariant form with isospin structure as [11]

$$\mathcal{L}_{eff}^{N} = \frac{G_F}{\sqrt{2}} \sum_{A,B,C,D} [j_\mu^A(\alpha_{AB}^{(0)} J_{(0)}^{B\mu} + \alpha_{AB}^{(3)} J_{(3)}^{B\mu}) + j^C(\alpha_{CD}^{(0)} J_{(0)}^{D} + \alpha_{CD}^{(3)} J_{(3)}^{D}) + j_{\mu\nu}(\alpha_T^{(0)} J_{(0)}^{\mu\nu} + \alpha_T^{(3)} J_{(3)}^{\mu\nu})], \quad (1)$$

(it refers to the nonphotonic μ-*e* mechanisms shown in Fig. 1). In Eq. (1) the symbols are $A, B = \{A, V\}$, $C, D = \{S, P\}$, with *S* standing for scalar, *V* for vector, *A* for axial-vector, *P* for pseudoscalar, and *T* for tensor interactions (the coefficients $\alpha_{lm}^{(k)}$ contain the couplings of the specific model [11]). The isoscalar $J_{(0)}$ and isovector $J_{(3)}$ nucleon currents are defined as

$$J_{(k)}^{V\mu} = \overline{N}\gamma^\mu \tau_k N, \quad J_{(k)}^{A\mu} = \overline{N}\gamma^\mu \gamma_5 \tau_k N, \quad J_{(k)}^{S} = \overline{N}\tau_k N, \quad (2)$$

$$J_{(k)}^{P} = \overline{N}\gamma_5 \tau_k N, \quad J_{(k)}^{\mu\nu} = \overline{N}\sigma^{\mu\nu}\tau_k N,$$

where $k = 0, 3$ and $\tau_0 \equiv \hat{I}$. The leptonic currents j_μ are described in Ref. [11].

Then the formulation of the nuclear $\mu^- \to e^-$ operators is usually done within the impulse approximation, by carrying out a multipole decomposition on the hadronic current-density matrix elements. This multipole analysis, assuming conserved vector current theory, leads to seven types of basic single-body multipole operators (they are denoted as $T_{i,M}^J$, $i = 1, 2, \ldots, 7$) [12]. These operators are given in terms of the projection functions

$$M_M^J(\mathbf{r}) = \delta_{LJ} j_L(\rho) Y_M^L(\hat{r}), \quad \mathbf{M}_M^{(L1)J}(\mathbf{r}) = j_L(qr)\mathbf{Y}_M^{(L1)J}(\hat{r}). \quad (3)$$

They involve the spherical Bessel functions $j_L(r)$ and the spherical Harmonics $Y_M^L(\hat{r})$ or the vector spherical Harmonics

$$\mathbf{Y}_M^{(L1)J}(\hat{r}) = \sum_{m,m'} \langle Lm1m' | JM \rangle Y_m^L(\hat{r}) \hat{q}_{m'}. \quad (4)$$

$\hat{r}$ and $\hat{q}$ are unit vectors in the directions of $\mathbf{r}$ and $\mathbf{q}$, respectively. The magnitude of the three-momentum transfer $|\mathbf{q}| = q$ is related to the nuclear excitation energy E_x as

$$q = m_\mu - \epsilon_b - E_x, \quad (5)$$

where m_μ is the muon mass, ϵ_b is the muon atomic binding energy and E_x is the excitation energy of the nucleus. Equation (5) shows that the $\mu^- \to e^-$ operators are strongly momentum dependent.

The matrix elements of the fundamental single-particle operators obtained from the decomposition procedure, T_i^{JM}, $1 = 1, 2, \ldots, 7$, in a harmonic oscillator basis can be cast in closed analytical forms as [12]

$$\langle j_1 \| \hat{T}^J \| j_2 \rangle = e^{-y} y^{\Lambda/2} \sum_{\mu=0}^{n_{max}} \mathcal{P}_\mu^J y^\mu, \quad y = (qb/2)^2 \quad (6)$$

where $j_i \equiv (n_i l_i) j_i$ and

$$n_{max} = (N_1 + N_2 - \Lambda)/2, \quad (7)$$

with

$$N_i = 2n_i + l_i.$$

The integer Λ that appears in Eqs. (6) and (7) depends on the specific operator T_i^{JM}. The coefficients $\mathcal{P}_\mu^J$ are, in general, simple rational numbers for the diagonal matrix elements of Eq. (6), and square roots of simple rational numbers for the nondiagonal ones [12].

B. The main ingredients of the DHF

The method employed in this work has comprehensively been discussed previously [21–23]. Here we provide in brief its essential ingredients required for our purposes. Assuming an axially symmetric nuclear regime, the construction of the many-body wave functions for the initial $|J_i^\pi\rangle$ and final $|J_f^\pi\rangle$ states needed for a partial μ-e conversion rate, proportional to matrix elements of the type,

$$\mathcal{M}_{i\to f} \sim |\langle J_f^\pi|\hat{O}_M^J|J_i^\pi\rangle|^2,$$

[the operators $\hat{O}_J^M$ are defined below in Eq. (13)] in the framework of the DHF proceeds with the following steps.

(i) At first, one chooses a model space consisting of a given set of single-particle orbits $|\lambda\rangle$ and the appropriate two-body effective interaction matrix elements.

(ii) By solving the axially symmetric HF single-particle equations self-consistently, the lowest-energy prolate (or oblate) intrinsic state (an antisymmetrized product of the HF orbits $|\lambda\rangle$ denoted as $|\chi_K\rangle$) for the nucleus in question is obtained.

(iii) The various excited intrinsic states $|\chi_K(\mu)\rangle$ are obtained by making particle-hole (p-h) excitations over the lowest-energy intrinsic state (lowest configuration) followed by a constrained HF calculation (tagged HF) for each of these states.

(iv) Then, because the HF intrinsic nuclear states $|\chi_K(\mu)\rangle$ do not have definite angular momenta, a projection on good angular momentum states $|\phi_{MK}^J(\mu)\rangle$ is required.

(v) Finally, for practical purposes one has, in general, to normalize the good angular momentum states $|\phi_{MK}^J\rangle$ for each J and obtain a set of orthonormalized vectors $|\Phi_M^J\rangle$.

In order to, furthermore, explain the above steps, we make now some additional remarks. Since the nucleus is assumed to be axially symmetric, each intrinsic state has a definite azimuthal quantum number K and is denoted by $|\chi_K(\mu)\rangle$, where the index μ counts the intrinsic states having the same K. Apparently, the states $|\phi_{MK}^J(\mu)\rangle$ are antisymmetrized products of the deformed single particle orbits $|\lambda\rangle$, which in our present work are chosen to be shell model orbits (see Sec. II C). As a consequence, they do not have definite angular momentum but they are linear combinations of states with good angular momentum.

States of good angular momentum are provided preferably via the projection method, i.e., by applying with the angular momentum projection operator

$$P_{MK}^J = \frac{2J+1}{8\pi^2}\int d\Omega D_{MK}^{J^*}(\Omega)R(\Omega) \tag{8}$$

on the intrinsic states $\chi_K(\eta)$, where $\Omega=(\alpha,\beta,\gamma)$ represent the Euler angles, $R(\Omega)$ represent the known general-rotation operator,

$$R(\Omega) = \exp(-i\alpha J_z)\exp(-i\beta J_y)\exp(-i\gamma J_z),$$

and the functions $D_{MK}^J(\Omega)$ are defined as

$$D_{MK}^J(\Omega) = \langle JM|R(\Omega)|JK\rangle.$$

The normalized states of good angular momentum J obtained via this procedure take the form

$$|\phi_{MK}^J(\eta)\rangle = \frac{2J+1}{8\pi^2\sqrt{N_{JK}}}\int d\Omega D_{MK}^{J^*}(\Omega)R(\Omega)|\chi_K(\eta)\rangle, \tag{9}$$

where N_{JK} is the normalization constant which (assuming axial symmetry) is given by

$$N_{JK} = \frac{2J+1}{2}\int_0^\pi d\beta \sin\beta d_{KK}^J(\beta)\langle\chi_K(\eta)|e^{-i\beta J_y}|\chi_K(\eta)\rangle. \tag{10}$$

The functions $d_{KK}^J(\beta)$ are the diagonal elements of the matrix $d_{MK}^J(\beta)=\langle JM|e^{-i\beta J_y}|JK\rangle$.

In the case when the overlap matrix constructed from the good angular momentum states $|\phi_{MK}^J\rangle$, i.e., the matrix

$$N_{K_1\eta_1,K\eta}^J = \langle\phi_{M_1K_1}^J(\eta_1)|\phi_{MK}^J(\eta)\rangle, \tag{11}$$

is nondiagonal [which means that $|\phi_{MK}^J(\eta)\rangle$ are nonorthogonal], a diagonalization of the matrix $N_{K_1\eta_1,K\eta}^J$ is carried out to give the orthonormal vectors $\Phi_M^J(\eta)$. Again, the index η distinguishes between different states having the same angular momentum J, by writing

$$|\Phi_M^J(\eta)\rangle = \sum_{K,\alpha} S_{K\eta}^J(\alpha)|\phi_{MK}^J(\alpha)\rangle.$$

For more details and explanations of the symbols, the reader is referred to Refs. [21–23].

It should be noted that in the DHF method one considers all low-lying intrinsic states in the band mixing calculations. In this way, the pairing correlations, which in other methods (RPA, QRPA, etc.) are explicitly taken into account, are included in the formalism.

C. The μ-e conversion matrix elements in the DHF

The deformed orbits $|\lambda\rangle$ entering the HF single-particle equations are expanded to a chosen (spherical) basis set of states $|j\rangle$. In the present work, the two-body interaction matrix elements are available in the shell model representation. For basis states $|j\rangle$ we use spherical harmonic oscillator shell model states as $|j\rangle\equiv|(nl)jk\tau\rangle$. In our axially symmetric solutions the orbits $|\lambda\rangle$ are eigenstates of the $\hat{J}_z$ operator and the latter expansion is limited to states with a given k_λ, so as we have

$$|\lambda\rangle = \sum_j c_{jk_\lambda}|jk_\lambda\tau_\lambda\rangle \tag{12}$$

where j denotes the (spherical) single-particle angular momentum and k_λ its projection along the symmetry axis (notice that k_λ is not summed over since this is a conserved quantity). In Eq. (12) the index τ_λ distinguishes proton and neutron orbits, but since μ-e conversion is a charge-preserving process, its operators do not mix proton and neutron states, and hence $|\lambda\rangle=\Sigma_j c_{jk_\lambda}|jk_\lambda\rangle$. The expan-

sion coefficients c_{jk_λ} are determined via the iterational procedure.

In the case of axially symmetric nuclear systems, the evaluation of the required reduced matrix elements of the μ-e conversion operators

$$\hat{O}_M^{(l,s)J} = \sum_{\lambda=1}^{n} \hat{T}_M^{(l,s)J}(\lambda), \tag{13}$$

where $n=Z(N)$, for proton (neutron) states, relies on the formula

$$\langle \phi_{K_1}^{J_1}(\mu) \| \hat{O}^{(l,s)J} \| \phi_{K_2}^{J_2}(\eta) \rangle = \frac{2J_2+1}{2} \sqrt{\frac{2J_1+1}{N_{J_1K_1} N_{J_2K2}}} \sum_{\nu} \begin{bmatrix} J_2 & J & J_1 \\ K_2 & \nu & K_1 \end{bmatrix} \times \int_0^{\pi} d\beta \sin\beta d_{K1,K2}^{J_1} \langle \chi_{K_1}(\mu) | e^{-i\beta J_y} \hat{O}_\nu^{(l,s)J} | \chi_{K_2}(\eta) \rangle. \tag{14}$$

In the latter equation, the square bracket [ ] represents the Clebsch-Gordon coefficient and the matrix element of the kernel is written as [22]

$$\langle \chi_{K_1}(\mu) | e^{-i\beta J_y} \hat{O}_\nu^{(l,s)J} | \chi_{K_2}(\eta) \rangle = \sum_{i,k=1}^{n} (-1)^{i+k} D_{i,k}^{n-1} \sum_{j_i,j_k} \frac{(-1)^{(3j_i - j_k - \nu)}}{(2j_k+1)^{1/2}} \times c_{j_i m_i}^{*} c_{j_k m_k} d_{m_i, m_k+\nu}^{j_i} \begin{bmatrix} j_i & J & j_k \\ m_k+\nu & -\nu & m_k \end{bmatrix} \times \langle (n_i l_i) j_i | \hat{T}_\nu^{(l,s)J} | (n_k l_k) j_k \rangle. \tag{15}$$

This can be proved [22] by noting that

$$\langle \chi_{K_1} | e^{-i\beta J_y} | \chi_{K_2} \rangle = \det[M_{il}(\beta)], \tag{16}$$

where

$$M_{il}(\beta) = \langle \lambda_i | \exp(-i\beta J_y) | \lambda_l \rangle = \sum_j c_{jk_i}^{*} c_{jk_l} d_{k_i k_l}^{j}(\beta). \tag{17}$$

In Eq. (15), $D_{i,k}^{n-1}$ stand for the determinants made of the matrix elements given by Eq. (17). They are determinants of rank $(n-1)$ obtained from the $n \times n$ determinant given in Eq. (16) by removing the ith row and kth column. The single-particle reduced matrix elements of the type $\langle j_i \| \hat{T}^{(l,s)J} \| j_k \rangle$ entering Eq. (15) are given in Eq. (6).

III. RESULTS AND DISCUSSION

Let us, first, describe shortly the calculational procedure followed in the context of DHF method [21] in order to obtain the low-lying spectrum.

A. Construction of the low-lying spectrum within DHF

The model space employed for the calculations comprises as active orbits the $1p_{3/2}$, $0f_{5/2}$, $1p_{1/2}$, and $0g_{9/2}$ single-particle levels, assuming that the ^{56}Ni nucleus plays the role of an inert core. The spherical single particle energies of these orbitals relative to ^{56}Ni are taken as 0.0, 0.78, 1.08, and 4.5 MeV, respectively (same for protons and neutrons). As effective interaction matrix elements in the region $A \sim 70$–80, several authors [21–23] used those of Kuo which have subsequently modified [23]. This effective interaction has been successfully used in describing many nuclear properties and important features of the nuclei in this region.

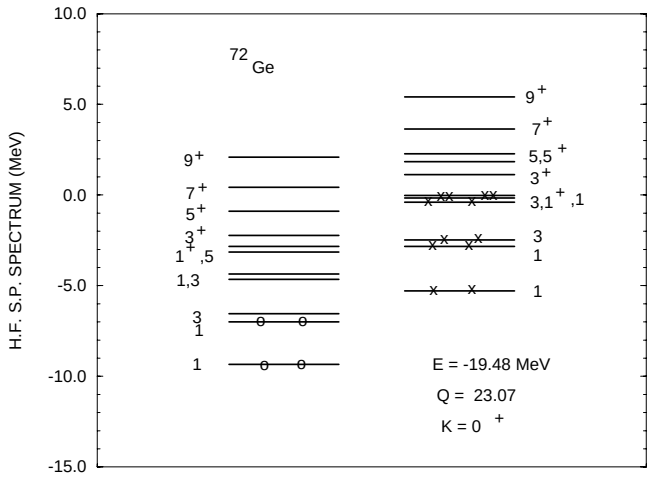

FIG. 2. The lowest prolate Hartree-Fock single-particle spectrum for ^{72}Ge. The single particle levels are characterized by twice the projection of the angular momentum to the symmetry axis of the nucleus ($2k_i$). The HF energy E is in MeV and the mass quadrupole moment Q is units of the square of the oscillator parameter b. In the notation $K=0^+$, the total K-quantum number of the intrinsic state is $K=\Sigma_i k_i=0$, where the sum runs over occupied states, and the parity is $\pi=+1$. Protons are represented by circles and neutrons by crosses.

The ground state (g.s.) of $^{72}_{32}$Ge in this method corresponds to the lowest 0^+ level obtained from the lowest $K=0^+$ intrinsic state.

The testing of the DHF g.s. wave function is illustrated in Fig. 2, where the lowest prolate Hartree-Fock single-particle spectrum for ^{72}Ge is shown. In this nucleus, the protons are distributed in the p-f single-particle orbits, but two neutrons occupy the g orbit (there is a gap of about 1 MeV above the neutron Fermi surface).

The good angular momentum states, which are projected out of this intrinsic HF state, are compared with the experimental levels of the ground state band in Fig. 3. We see that, with the exception of the $2^+ \rightarrow 0^+$ separation (its difference from the experimental value may be due to the nonexplicit consideration of pairing correlations), the relative energies of all the levels agree reasonably well with experiment. We have considered only the levels up to $J=6^+$. For levels with $J=8^+$ and higher the angular momentum alignment effects become important and one should carry out full spectroscopic calculations. On the other hand, for studying the transition matrix elements of the exotic (μ^-, e^-) conversion process, such high-lying levels are, in general, not important [15] (except the dipole and spin-dipole resonances which, however, cannot be studied with our restricted model space).

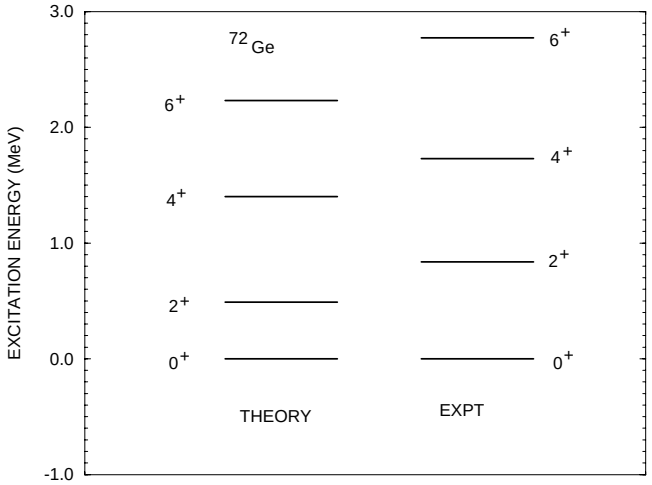

FIG. 3. Theoretical and experimental ground state band spectrum of the ^{72}Ge nucleus. These levels correspond to the lowest $K=0^+$ intrinsic state.

In addition to the ground state band, we have considered the following four excited intrinsic positive parity states.

(1) One excited intrinsic state with $K=0^+$ is obtained by promoting two valence protons to $k=3/2^-$ orbital and then performing a "tagged" HF calculation in which the occupancy of these two protons is held fixed and for the rest of the particles a self-consistent HF calculation is performed.

(2) We have considered two excited intrinsic states, one with $K=1^+$ and the other with $K=2^+$, produced by the excitation of a valence proton to the $k=3/2^-$ level and then performing a "tagged" HF calculation.

(3) We have obtained another $K=2^+$ excited intrinsic state, by exciting a neutron from $k=1/2^+$ orbit to $k=3/2^+$ orbit. Good angular momentum states are projected from each of these intrinsic states and these good angular momentum states are used for evaluating the μ-e conversion matrix elements discussed below (see Sec. III C).

In our model space we can also obtain negative parity intrinsic bands (their contribution to μ-e strengths in QRPA calculations was found to be very important [18]) in two ways: by exciting either a neutron or a proton from p-f orbit to $g_{9/2}$ orbit. The negative parity intrinsic band obtained by exciting a proton to $g_{9/2}$ orbital lies high in energy, at around 5 MeV. The neutron excited negative parity band lies at about 2.2 MeV. In each of the above cases tagged HF calculation is carried out to obtain the excited intrinsic states.

In summary for our calculation we consider the following bands.

(i) The lowest $K=0^+$ band, which gives on angular momentum projection the lowest $J=0^+, 2^+, 4^+$, etc., levels.

(ii) The first excited $K=0^+$ intrinsic band, which on angular momentum projection gives also the excited levels $J=0^+, 2^+, 4^+$, etc.

(iii) Two $K=2^+$ intrinsic bands obtained, respectively, by neutron and proton excitation. These intrinsic bands give the excited $J=2^+, 3^+, 4^+$, etc., levels of the γ band.

(iv) The $K=1^+$ intrinsic band, which gives the levels $J=1^+, 2^+, 3^+$, etc. None of these levels has been observed even though they appear in the theoretical spectrum at an excitation energy about 1 MeV.

(v) One $K=1^-$ negative parity band, which on angular momentum gives the levels $J=1^-, 2^-, 3^-, 4^-, \ldots$. As discussed earlier, this band is obtained by exciting a valence neutron from p-f orbit to $g_{9/2}$ orbit. These levels lie at an excitation of about 2.2 MeV.

(vi) One $K=0^-$ intrinsic band, which is obtained by promoting a valence proton from p-f orbit to $g_{9/2}$ orbit. The projected levels of this band lie very high in energy, at around 5 MeV. Experimentally a negative parity band has not been observed for this nucleus. However some negative parity levels have been identified at an excitation of around 2.5 MeV.

B. Coherent μ-e matrix elements

The coherent mode is the only potentially measured directly μ-e conversion channel (its rate is currently measured at the SINDRUM II [6] and MECO [8,9] detectors and is expected to be measured in the future PRIME experiment at KEK (Japan) [10,20]). Also, on the theoretical side, mostly the coherent contribution is employed for the estimation of the branching ratio $R_{\mu e}$. It is utilized in combining nuclear physics input with experimental limits on $R_{\mu e}$, to put constraints on the LFV parameters entering the μ-e conversion effective currents in modern gauge theories [11,20].

The scalar and vector g.s.$\rightarrow$g.s. transition matrix elements, if the corresponding couplings of the prevailing mechanism in μ-e conversion are known to a rather good approximation (depending on the properties of the nuclear target), can be determined by the proton (F_Z) and neutron (F_N) nuclear form factors [25]. In Table I, we quote the results for F_Z and F_N of ^{72}Ge obtained with the deformed HF (present work) and compare them with the results of (i) the

TABLE I. Proton F_Z and neutron F_N nuclear form factors, obtained with "spherical" and "deformed" models in the case of ^{72}Ge nucleus. The corresponding coherent matrix elements for the μ-e conversion in photonic (γ-exchange) and nonphotonic (W-exchange) mechanism are also shown.

^{72}Ge	Expt.	Independent particle SM	QRPA [16]	RQRPA [16]	DHF (this work)
$b_{\text{h.o.}}$ (fm)		2.04	2.07	2.07	1.90
F_Z	0.443	0.456	0.472	0.441	0.449
F_N		0.435	0.451	0.422	0.429
$M^2_{\text{coh}}(\gamma-\text{exc})$	200.9	212.9	169.9	199.1	206.0
$M^2_{\text{coh}}(W-\text{exc})$		595.8	477.1	558.9	623.2

TABLE II. Incoherent transition matrix element of the $T^{(l,\sigma)J}$ operators for selected spin-isospin combinations. States not appearing in the first column contribute less than 10^{-3} for all components.

	DHF excited states	Photonic mechanism	Nonphotonic mechanism	
J^π	Origin	Vector	Vector	Axial-vector
2^+	Lowest $K=0^+$ g.s. band	0.997	6.245	0.0002
2^+	γ band			0.035
4^+	γ band	1×10^{-5}	0.001	
0^+	First excited $K=0^+$ band	4×10^{-4}	0.006	
2^+	γ band	0.114	0.438	
4^+	γ band	0.001	0.005	
2^+	$K=1^+$ band	0.018	0.073	0.005
3^+	$K=1^+$ band			0.011
4^+	$K=1^+$ band		2×10^{-4}	0.0002
3^-	Band (v)	0.0	0.001	1×10^{-5}
2^-	Band (vi)	0.016		0.178
3^-	Band (vi)	0.016	0.057	0.003
4^-	Band (vi)	0.016		0.0002
Total		1.157	6.826	0.201

independent particle shell model calculations using a single Slater determinant [24], (ii) the normal QRPA [15], and (iii) the renormalized QRPA [16] (previous works). We see that the proton and neutron nuclear form factors agree rather well among each other and with experiment. It is, however, worthwhile noting that, in DHF the h.o. size parameter b is treated rather as a parameter determined by the variational procedure and not obtained by the known semiempirical formulas (see discussion in Refs. [15,18]) as is the case in other methods. The value obtained, $b=1.90$ fm, is quite smaller than those of the other methods and slightly different than that given by the standard $A^{1/6}$ parametrization. If in DHF we use the value of RPA and QRPA calculations [15,18], $b=2.07$ fm^{-1} (see Table I), at $q=m_\mu-\epsilon_b=0.525$ fm^{-1} (the coherent momentum transfer of ^{72}Ge), we obtain proton and neutron form factors equal to $F_Z=0.392$ and $F_N=0.371$, respectively, values which are not in good agreement with the experimental data. Subsequently, the obtained in DHF coherent matrix elements are appreciably smaller than those corresponding to the value $b=1.90$ fm.

In Table I, the coherent matrix elements M^2_{coh} of the present DHF calculations and those of Ref. [15,16,24] refer to the photonic and W-boson exchange (nonphotonic) mechanisms. As can be seen, the results of DHF for the γ-exchange process lie in-between those given by the other methods [15,16,24], but those for the W-exchange mechanisms are a bit larger. Since, neutrons do not participate in the photonic mechanism, the DHF method gives (for ^{72}Ge) a larger neutron contribution compared to other methods. We should mention, however, that, the neutron contribution for the photonic diagrams is assumed to be zero by definition of the specific isospin dependence of the vector-type operator in the μ-e process, which (at the quark level) is determined by the ratio of isovector to isoscalar couplings [parameter β of Eq. (2) of Ref. [13])]. The axial vector contribution is vanishing for the 0^+ g.s. of the even-even ^{72}Ge nucleus.

C. Incoherent μ-e matrix elements

In this work we performed detailed calculations for the dominant μ-e matrix elements (scalar, vector, and axial vector). Extensive results including contributions from other operators (for isotopes in the region $30\leqslant Z\leqslant 60$, where the branching ratio $R_{\mu e}$ takes the largest value [20]) will be provided by applying special QRPA treatments elsewhere [26].

The incoherent μ-e matrix elements are of the form

$$S_\alpha=\sum_f\left(\frac{q_f}{m_\mu}\right)^2\int\frac{d\hat{\mathbf{q}}_f}{4\pi}|\langle J^\pi_\lambda, M|\Omega_\alpha|\text{g.s.}\rangle|^2, f\equiv(J^\pi_\lambda, M). \tag{18}$$

In S_α (S_S for the scalar, S_V for the vector and S_A for the axial vector operators Ω_α [13,14]) partial contributions coming from all excited states produced by our DHF model space are summed over. Since the $|\text{g.s.}\rangle$ of ^{72}Ge nucleus corresponds to the lowest 0^+ level obtained from the lowest $K=0^+$ intrinsic state, one important category of the states $|f\rangle$ will correspond to the excited levels projected from this $K=0^+$ intrinsic state. The states $|f\rangle$, however, can in addition be deduced from the good angular momentum states projected out of other excited intrinsic states. In Table II, the incoherent matrix elements listed represent the sum of the contributions of all states (with energies up to about 5 MeV and spin up to $J^\pi=6^+$) produced as described in Sec. III A. We see that the main incoherent rate originates from the excitations of the g.s. band and that the maximum contribution comes from the first excited state, a 2^+ state that is reproduced very well, at the experimental energy value by our DHF model.

An interesting feature comes out of the calculated strengths for negative parity bands. In previous RPA calculations, such excitations (especially the 1^- states) provided a great portion of the incoherent rate. In the DHF results, the

TABLE III. Deformed HF results for coherent, incoherent ($M^2_{\rm inc}=S_V+3S_A$) and total ($M^2_{\rm tot}=M^2_{\rm coh}+M^2_{\rm inc}$) matrix elements in $^{72}_{32}$Ge. The photonic and W-exchange diagrams are included.

Mechanism	S_V(coh)	S_A(coh)	$M^2_{\rm coh}$	S_V(inc)	S_A(inc)	$M^2_{\rm inc}$	$M^2_{\rm tot}$
γ exchange	206.0		206.0	1.2		1.2	207.2
W exchange	623.2		623.2	6.8	0.2	7.0	630.2

contribution of all negative parity states included in the truncated model space differs significantly from that obtained by RPA methods. This may be attributed to the following reasons. The spherical $f_{7/2}$ orbital, which does not contribute to the spectroscopic properties of nuclei in the region of Ge isotopes [21], is not included in our valence space. Thus, several 1^- states, which in RPA methods may give significant incoherent matrix elements, are not constructed in our DHF model. Essentially, the rate that proceeds via the negative parity excitations in the present calculations comes from the $K=1^-$ band [case (v) of Sec. III A]. The only $J^\pi=1^-$ state included into the sum of Eq. (18) is the one produced when a neutron from the $g_{9/2}$ orbit is excited (that produced when a proton is excited from the $g_{9/2}$ orbit lies much higher). This is why the comparison with RPA results is worst for the photonic mechanism (only protons contribute) than for the nonphotonic one (see Table III). The general characteristics of the DHF transition matrix elements resemble the (spherical) shell model ones [13,14] where also reduced model space was used (in the case of s-d shell model results for ^{27}Al [13] the negative parity contributions are not estimated).

At this point, we find it interesting for the reader to shortly discuss the main features of our present method in conjunction with the advantages and drawbacks of various methods employed up to now to investigate the incoherent μ-e rate. Up to now, transition rates to excited nuclear states for the μ-e reaction have been studied by employing several methods.

(i) Closure approximation (in the context of the independent particle shell model [24] and QRPA [15]) which provides the average total rate to all excited states (including the continuum spectrum) of the final nucleus [15].

(ii) Relativistic Fermi gas approach utilizing a relativistic Lindhard function to compute the average incoherent rate for a nuclear matter system followed by a projection into finite nuclei via a local density approximation [27].

(iii) Sum over partial transition strengths evaluation (state-by-state calculations) of the incoherent rate.

The excited nuclear states are explicitly constructed by utilizing reliable nuclear structure models such as the QRPA, shell model, etc. [13–15].

The method used in the present paper belongs to the latter category. From the above description it becomes clear that methods (i) and (ii) may estimate the part of the rate that goes to the continuum but they are not appropriate for evaluating the individual contribution of each accessible channel. On the other hand, RPA, QRPA, shell model (SM), DHF, etc., offer the possibility of detailed term-by-term investigation of the individual (μ^-, e^-) conversion channels included in a chosen valence space. Obviously, the contribution of the continuum spectrum, which includes the giant dipole resonances, could hardly be studied within methods such as the usual SM, ordinary RPA, as well as in our DFH method. It could, for example, be studied in the context of the continuum RPA [28] or the large scale shell model calculations developed recently [29]. The latter method was used very successfully in the study of stable and exotic nuclei in the region of Ge isotopes (fp and fpg shell nuclei) using as inert core either ^{48}Ca or ^{56}Ni as is our case here [30,31]. Such detailed calculations may shed light on the question of the level of spuriosity of the 1^- multipole states. For RPA methods the 1^- states contribute a great portion into the total incoherent μ-e rate, but recently it has been found by Bes and Civitarese [19] that this contribution for some nuclear systems is rather fully spurious.

As is known, spectroscopic calculations like our transition matrix elements of Eq. (18), which rely on an inert core, consider effective charges for protons (e_p) and neutrons (e_n). Since, there are no methods of calculating them starting from first principles, they have to be fitted or adjusted. Thus, their values depend on the effective interaction and the active model space used. In previous calculations [21] performed with the modified Kuo interaction in the $f_{5/2}pg_{9/2}$ valence space, i.e., same as in the present work, the effective charges $e_p=1.6e$ and $e_n=1.0e$ have been used for all nuclei in the upper p-f shell. These effective charges satisfactorily explain the $B(E2)$ values of a large number of nuclei in this region [21]. In the present calculations of the transition strengths for ^{72}Ge use of the above values for the effective charges e_p and e_n has been done both for photonic and W-exchange mechanisms.

Before closing it is worth mentioning that the shape of a nucleus is unambiguously determined from the measurement of the static quadrupole moment. In the $A\sim80$ region, such measurements are quite difficult. In Ref. [32], the calculated quadrupole deformation parameter for ^{72}Ge was found to be $\beta=-0.214$, which corresponds to an oblate nuclear shape. However, if one follows this theoretical result assuming that the shape of the nucleus ^{72}Ge is oblate, the description of the spectroscopic data is very poor compared to the prolate case. Furthermore, this is, in addition, not supported by the fact that the only nucleus for which there is some indirect experimental evidence regarding oblate shape is the ^{68}Se nucleus [33]. For this reason, we assume a prolate shape for ^{72}Ge, and in Fig. 2 we present the lowest prolate single-particle energies.

IV. SUMMARY AND CONCLUSIONS

We have calculated the low-lying spectrum of $^{72}_{32}$Ge nucleus in the context of a deformed configuration mixing shell model method based on Hartree-Fock states by using as

two-body interaction the modified Kuo effective interaction for the $f_{5/2}pg_{9/2}$ valence space. Using these axially deformed HF wave functions, we have performed calculations for the coherent and incoherent $\mu^- \rightarrow e^-$ transition matrix elements of the ^{72}Ge nucleus. This moderately deformed isotope lies in the region of the periodic table where the branching ratio $R_{\mu e}$ takes the largest value.

From comparison with previous results of the literature where the nuclear deformation was not considered in ^{72}Ge, we conclude the following. In the description of the coherent $\mu^- \rightarrow e^-$ channel all methods do not show appreciable differences. However, in the case of the incoherent rate the DHF gives very small matrix elements especially in the case of the photonic mechanism. This is mainly due to the fact that the treatment of this nucleus and the spectra derived by DHF and RPA methods are different. Also, the model space of QRPA calculations is much larger than that of the DHF, so that a state-by-state comparison of the incoherent contributions obtained by the two methods cannot be directly done for all accessible individual channels.

The fact that the interaction used in the present DHF calculations is well tested in the region of Ge isotopes provides us with quite high confidence about the obtained results for the low-lying transitions induced by the μ-e operators. However, detailed calculations for transitions to higher excitations not derived by our reduced model space and especially to the continuum spectrum (including the giant dipole and spin dipole resonances) are still needed. This requires special treatment (e.g., large scale shell model, continuum RPA, etc.) due to the high sensitivity of the $\mu^- \rightarrow e^-$ matrix elements and its use as input to severely constrain the parameter space of elementary models predicting LFV processes.

ACKNOWLEDGMENTS

This work was supported in part by the Europäisches Gratuiertenkolleg Basel-Tübingen and the IKY-DA-02 project (T.S.K.).

[1] P. Scheck, Phys. Rep. **44**, 187 (1979).
[2] Y. Kuno and S. Okada, Rev. Mod. Phys. **73**, 151 (2001).
[3] J. Suhonen and O. Civitarese, Phys. Rep. **300**, 123 (1998).
[4] T. S. Kosmas, Nucl. Phys. **A683**, 443 (2001).
[5] T. S. Kosmas, Invited talk at 3rd International Workshop on Neutrino Factories based on Muon Storage Rings, NuFACT'01, Tsukuba, Japan, 2001 [Nucl. Instrum. Methods Phys. Res. A **503**, 247 (2003)].
[6] Prog. Part. Nucl. Phys. **31**, 1 (1993); the SINDRUM II invited talk at [5].
[7] P. Wintz, in Proceedings "Honolulu 2000," Status of μ-e conversion at PSI, invited talk at Workshop on New initiatives in LFV and ν-oscillations with very intense muon and neutrino beams, edited by Y. Kuno, W. R. Molzon, and S. Pakvasa (World Scientific, Singapore, 2002), p. 72.
[8] W. Molzon, Springer Tracts Mod. Phys. **163**, 105 (2000).
[9] J. Sculli, the MECO experiment, invited talk at [7].
[10] M. Aoki, the PRIME experiment, invited talk at [5].
[11] A. Faessler, T. S. Kosmas, S. Kovalenko, and J. D. Vergados, Nucl. Phys. **B587**, 25 (2000); T. S. Kosmas, S. Kovalenko, and I. Schmidt, Phys. Lett. B **511**, 203 (2001); **519**, 78 (2001); F. Šimkovic *et al.*, *ibid.* **554**, 121 (2002).
[12] T. S. Kosmas, Prog. Part. Nucl. Phys. **48**, 307 (2002); V. Ch. Chasioti and T. S. Kosmas, Czech. J. Phys. **52**, 467 (2002); nucl-th/0202062.
[13] T. Siiskonen, J. Suhonen, and T. S. Kosmas, Phys. Rev. C **60**, 062501(R) (1999).
[14] T. Siiskonen, J. Suhonen, and T. S. Kosmas, Phys. Rev. C **62**, 035502 (2000).
[15] T. S. Kosmas, J. D. Vergados, O. Civitarese, and A. Faessler, Nucl. Phys. **A570**, 637 (1994); T. S. Kosmas, A. Faessler, F. Šimkovic and J. D. Vergados, Phys. Rev. C **56**, 526 (1997).
[16] J. Schwieger, T. S. Kosmas, and A. Faessler, Phys. Lett. B **443**, 7 (1998); T. S. Kosmas, Z. Ren, and A. Faessler, Nucl. Phys. **A665**, 183 (2000).
[17] J. Toivanen and J. Suhonen, Phys. Rev. Lett. **75**, 410 (1995).
[18] J. Schwieger, A. Faessler, and T. S. Kosmas, Phys. Rev. C **56**, 2830 (1997).
[19] D. R. Bes and O. Civitarese, Phys. Rev. C **63**, 044323 (2001).
[20] R. Kitano, M. Koike, and Y. Okada, Phys. Rev. D **66**, 096002 (2002).
[21] R. Sahu, D. P. Ahalpara, and S. P. Pandya, J. Phys. G **13**, 603 (1997); K. C. Tripathy and R. Sahu, *ibid.* **20**, 911 (1994); Nucl. Phys. **A597**, 177 (1996); K. C. Tripathy, R. Sahu, and S. P. Pandya, J. Phys. G **23**, 433 (1997).
[22] R. Sahu and S. P. Pandya, Nucl. Phys. **A414**, 240 (1984); J. Phys. G **14**, L165 (1988); Nucl. Phys. **A529**, 20 (1991); **A571**, 253 (1994); R. Sahu, F. Šimkovic, and A. Faessler, J. Phys. G **25**, 1159 (1999).
[23] R. Sahu and V. K. B. Kota, Phys. Rev. C **66**, 024301 (2002); **67**, 054323 (2003).
[24] T. S. Kosmas and J. D. Vergados, Phys. Lett. B **217**, 19 (1989); Nucl. Phys. **A510**, 641 (1990); Phys. Rep. **264**, 251 (1996).
[25] T. S. Kosmas and I. E. Lagaris, J. Phys. G **28**, 2907 (2002).
[26] Ch. C. Moustakidis *et al.* (unpublished).
[27] H. C. Chiang, E. Oset, T. S. Kosmas, A. Faessler, and J. D. Vergados, Nucl. Phys. **A559**, 526 (1993).
[28] E. Kolbe and T. S. Kosmas, Springer Tracts Mod. Phys. **163**, 199 (2000).
[29] E. Caurier, F. Nowaki, A. Poves, and J. Retamosa, Phys. Rev. Lett. **77**, 1954 (1996).
[30] J. M. Daugas *et al.*, Phys. Lett. B **476**, 213 (2000).
[31] O. Kenn, K.-H. Speidel, R. Ernst, S. Schielke, S. Wagner, J. Gerber, P. Maeir-Komor, and F. Nowaki, Phys. Rev. C **65**, 034308 (2002).
[32] G. A. Lalazissis, S. Raman, and P. Ring, At. Data Nucl. Data Tables **71**, 1 (1999).
[33] S. M. Fischer *et al.*, Phys. Rev. Lett. **84**, 4064 (2000).